Macromolecules
ARTICLE

Macromolecules **2010**, *43*, 3365–3375 **3365**
DOI: 10.1021/ma902584z

Variation of Lattice Parameters with Fold State in the Ultralong *n*-Alkanes

Timothy D. Lord,[†,§] Jamie K. Hobbs,[‡] Ann E. Terry,[⊥] Åke Kvick,[§] and Simon Hanna*[,†]

[†]*H.H. Wills Physics Laboratory, University of Bristol, Tyndall Avenue, Bristol BS8 1TL, U.K.,* [‡]*Departments of Physics & Astronomy and Chemistry, University of Sheffield, Western Bank, Sheffield S10 2TN, U.K.,* [§]*Beamline ID11, ESRF, 6 rue Jules Horowitz, BP220, 38043 Grenoble Cedex, France, and* [⊥]*ISIS Science Diffraction & Muon Division, CCLRC Rutherford Appleton Laboratory, Chilton, Didcot, Oxfordshire OX11 0QX, U.K.*

Received November 23, 2009; Revised Manuscript Received February 27, 2010

ABSTRACT: The ultralong *n*-alkanes were synthesized to provide model materials for the study of polyethylene chain folding and crystallization. In this paper, results are presented from a detailed wide- and small-angle X-ray diffraction study of these materials, which have been crystallized in a range of different fold states. The trends in lattice parameter are quantified as a function of temperature, lamellar thickness, and the number of folds in each chain. For a given lamellar thickness, it is found that the unit cell expands with increasing number of chain folds. However, when the number of folds is kept constant, a contraction in the unit cell is observed on increasing the lamellar thickness, and an approximate inverse relationship exists between the *a* lattice parameter of the unit cell and the lamellar thickness. Above ca. 70 °C, increases are observed in the thermal expansion coefficients of the *a* lattice parameters, which appear to be associated with an α relaxation process in the *n*-alkane crystals. This relaxation process also appears to be related to the onset of chain tilting in the lamellae. It is found that almost all samples melt, or undergo unfolding transitions, when the *a* lattice parameter reaches a critical value in the range 7.660 ± 0.005 Å. This value appears to mark an upper limit for the free volume in the unit cell, above which the crystals cease to be stable. The melting temperatures of the extended-chain crystals are shown to be consistent with predictions of the Flory−Vrij equation. By introducing an additional free energy term into the Flory−Vrij analysis, it is also possible to account for the unfolding temperatures of the folded-chain *n*-alkane crystals.

1. Introduction

Many polymer crystals display an unstable, "nonequilibrium" nature, and this gives them their unique properties. The crystallization of flexible polymers is governed by kinetics. With few exceptions, flexible polymers consist of a mixture of molecular chains of different lengths and crystallize into thin platelike lamellae, often containing high levels of defects and varying considerably in thickness. This high defect level sets polymer crystals apart from low molar mass systems. The lamellar thickness depends on the precise conditions of crystallization, and subsequent annealing can lead to crystal thickening. The crystalline lattice parameters may vary with lamellar thickness, and as a consequence of this, they will also depend on the thermal history of the sample. These features make the study of the mechanisms of polymer crystallization, and the subsequent crystalline structure, quite challenging.

In order to address this subject, a series of monodisperse ultralong *n*-alkanes, with backbones containing up to 390 carbon atoms, were synthesized to act as model materials for the study of the crystallization of polyethylene.[1,2] Given appropriate crystallization conditions, the ultralong *n*-alkanes form extremely regular crystals with lamellar populations that possess very narrow thickness distributions and hence similar stabilities. These crystals generally possess well-defined fold surfaces due to the fact that all the chains in the crystal have the same molecular weight and all fold at the same point. Different fold states are possible by varying the crystallization temperature and time. For example, it is possible to produce crystals with 0, 1, 2, or 3 folds per molecule and an approximate lamellar thickness $L/(m + 1)$, where L is the length of the *n*-alkane, and there are m folds per alkane molecule.[3−6] These are referred to as integer folded crystals. Under certain crystallization conditions, more disordered structures are formed, in which the lamellar thickness does not correspond to an integer number of folds. These noninteger folded (NIF) materials have been studied extensively elsewhere.[7,8] A comprehensive review of the crystallization and morphology of the ultralong *n*-alkanes may be found in the literature.[9]

The crystal structure of polyethylene has been reported many times.[10−17] The classical structure is that of Bunn from 1939,[10] which was actually derived from long *n*-alkanes. Bunn found an orthorhombic unit cell (space group *Pnam*, 2 chains per cell) with $a = 0.740$ nm, $b = 0.493$ nm, and $c = 0.2534$ nm. These, or similar, lattice parameters are sometimes used as a starting point for molecular modeling projects involving polyethylene.[18−21] However, considerable variability is observed in the published lattice parameters, with the precise values dependent on sample preparation and thermal history. Systematic studies of this dependence were conducted by Davis et al.[22,23] In those studies, solution and melt-crystallized polyethylene samples were probed using wide- and small-angle X-ray diffraction. It was found that, for a given polyethylene sample, the unit cell dimensions are not unique but vary systematically with crystallization conditions, annealing, and deformation. Moreover, it was shown that the *a* and *b* lattice parameters vary linearly with the reciprocal of lamellar thickness at room temperature; i.e., lamellae that were less extended parallel to the chain axis direction (*c* axis) of the unit cell gave rise to unit cells that were expanded perpendicular to that direction.

*Corresponding author: Tel +44 (0)117 928 8771; Fax +44 (0)117 9255624; e-mail s.hanna@bristol.ac.uk.

Published on Web 03/05/2010

Performing such measurements on polyethylene crystals is technically challenging; each sample contains a distribution of lamellar thicknesses, and the poor resolution wide-angle X-ray scattering data that are available make it difficult to separate the crystalline and amorphous phases, so that lattice parameter determination can be unreliable. The advent of the ultralong *n*-alkanes creates the possibility of studying the influence of lamellar thickness on unit cell parameters in a more controlled fashion, since each ultralong *n*-alkane sample has a sharply defined lamellar thickness dependent on the chain length and number of folds.

Interestingly, lamellar thickening occurs on heating the ultralong *n*-alkanes, just as in the polymeric case. However, in contrast to the gradual thickening observed in populations of polyethylene crystals, the ultralong *n*-alkanes thicken in a series of discrete stages, at well-defined temperatures, corresponding to a stepwise unfolding of the molecules.[3−6,24,25] During this process, lamellae possessing two folds per chain, for example, will first undergo a transition to one fold per chain and then to a fully extended configuration. Therefore, studying the crystal structure of *n*-alkane crystals affords the opportunity to examine not only the effects of temperature, lamellar thickness, and polymer chain length on the lattice parameters but also the influence of different fold states.

In a previous paper, solution-grown *n*-alkane crystals were studied using high-temperature wide-angle X-ray diffraction (WAXD) on the Materials Science beamline ID11 at the European Synchrotron Radiation Facility (ESRF) in Grenoble.[26] The unfolding transitions described above were observed, and in each case, there appeared to be an associated contraction in the *a* and *b* lattice parameters. However, the resolution of the study was insufficient to establish a quantitative relationship between the lattice dimensions and the lamellar thickness. In addition, the *c* parameter of the unit cell was not determined, and there was no measurement of the crystalline density.

In the present paper we address these shortcoming by reporting the results of a high-resolution WAXD study of the same materials. Powder diffraction data were obtained on beamline ID11 at the ERSF for a range of ultralong *n*-alkane samples as they were heated to the melt. These data were supplemented by small-angle X-ray scattering (SAXS) measurements on beamline ID2 which confirmed the lamellar thicknesses and hence the fold states. We report precise lattice parameters for each material and discuss the trends observed as a function both of the temperature and of the fold state of the material. Also, we examine the conditions under which chain-unfolding occurs and establish a criterion for the process based on a critical lattice parameter for the material. This work is supplemented by a brief study of lattice parameter variation during crystallization from the melt. A discussion of the structural changes within the unit cell, and of the effect of pressure on the lattice parameters, will be reserved for a later publication.

2. Experimental Method

2.1. Materials and Sample Preparation. Seven *n*-alkanes were investigated, with backbones ranging from 102 to 390 carbon atoms. Their chemical formulas and available fold states are listed in Table 1. These materials were synthesized by Brooke et al.[2] and were provided by the Engineering and Physical Sciences Research Council (EPSRC) of the UK. The *n*-alkanes were crystallized into their appropriate crystal form, from dilute solution in toluene.[27] Further details are given in the Supporting Information. After removal of the solvent, the crystalline powder was transferred into 0.5 mm diameter Lindemann glass capillaries.

Two further alkane samples were also investigated, with side branches in the middle of the chain and chemical formula: $C_{96}H_{193}CH(R)C_{94}H_{189}$. In these materials, the branches are either "long" butyl branches (R = $(CH_2)_3CH_3$) or "short" methyl branches (R = CH_3), and the position of the branch corresponds to the fold point of a once-folded system. In terms of the *n*-alkanes, these branched materials most closely match the lengths of $C_{198}H_{398}$. However, the presence of the branch is expected to favor the formation of once-folded crystals.[28,29] Since the alkanes are viewed as a model material for polymers, it is important to compare the results to those obtained from polyethylene. For this purpose, a high-density commercial polyethylene, Rigidex 50 (B.P. Chemicals Ltd.), was examined. Rigidex 50 has a molecular weight of $M_n = 7 \times 10^4$ and polydispersity of 7.

Table 1. A Summary of the Alkane Samples Included in This Study, Indicating Their Initial Fold States and Sample Labels

material	extended chain	once-folded	twice-folded	thrice-folded
$C_{102}H_{206}$	C102:e			
$C_{122}H_{246}$	C122:e			
$C_{162}H_{326}$	C162:e			
$C_{198}H_{398}$	C198:e	C198:1f		
$C_{246}H_{494}$	C246:e	C246:1f		
$C_{294}H_{590}$		C294:1f	C294:2f	
$C_{390}H_{782}$			C390:2f	C390:3f
$C_{96}H_{193}CH(CH_3)C_{94}H_{189}$		C191:Me		
$C_{96}H_{193}CH(C_4H_9)C_{94}H_{189}$		C191:Bu		

2.2. X-ray Measurements. The WAXD study was performed on the Materials Science beamline, ID11, at the ESRF in Grenoble. For the heating runs, each capillary was mounted in a holder on the front face of a silver block Linkam TMS600 hot stage and heated from 25 to 140 °C at 2 °C/min. The Linkam heater and data collection were controlled using the commercial software package, SPEC (Certified Scientific Software). Wide-angle diffraction patterns were collected using a Bruker 6500 CCD camera. Images with dimensions of 2048 × 2048 pixels, and a pixel size of 70 μm, were collected every 18 s, giving one frame every 0.6 °C. The X-ray wavelength was 0.5166 Å, i.e., an energy of 24 keV. The beam size was 300 μm × 300 μm. The beam shutter was closed between exposures to minimize radiation damage to the sample. High-resolution WAXD patterns were obtained with *d*-spacings in the range of 0.96 Å < d < 12.33 Å (2.4° < 2θ < 31.2°). The lower limit of *d* was chosen to ensure that the *c* axis repeat, i.e. the (002) reflection, was captured by the detector.

A complementary set of SAXS measurements were performed on the high brilliance beamline ID2 at the ESRF. Small-angle data were collected using an XRII-FReLoN CCD camera.[41] Images with pixel array dimensions 1024 × 1024, and pixel size of 163.5 μm, were collected every 15 s, hence giving one frame every 0.5 °C. The sample detector distance was calibrated using orders from a standard specimen of silver behenate. The X-ray wavelength used was 0.995 Å, energy 12 keV. The beam size was 100 μm × 100 μm. Patterns with a q range of 0.009 Å^{-1} < q < 0.125 Å^{-1} (corresponding to *d*-spacings in the range 50 Å < d < 700 Å) were collected. The sample−detector distance was 5 m.

Crystallization experiments were performed on samples of $C_{246}H_{494}$ only. In the first set of experiments, samples were heated to the melt (140 °C) at 25 °C/min, without recording data. Then, WAXD patterns were collected as the material was cooled at 1 °C/min to 100 °C and then reheated to the melt at 2 °C/min. In a second experiment, a sample of $C_{246}H_{494}$ was heated to the melt without recording data at 25 °C/min, cooled at 2 °C/min to 128.1 °C, and then held at that temperature for 30 min while WAXD patterns were collected to observe isothermal crystallization.

2.3. Sample−Detector Distance. For the WAXD measurements, the sample−detector distance was calibrated with a sample of alumina (Al_2O_3). This resulted in a calibrated sample−detector

Table 2. Errors in Lattice Parameters Measured for a Sample of Once-Folded $C_{246}H_{494}$, Determined Using Variations in the Sample−Detector Distance and Resulting from the Rietveld Refinement

	±Δ*a* (Å)	±Δ*b* (Å)	±Δ*c* (Å)
error due to variation in sample placement	0.002	0.0009	0.0005
standard Rietveld refinement error	0.0004	0.0003	0.0001

distance of 140.13 ± 0.03 mm (see Supporting Information for further experimental details). The error in the sample−detector distance for each sample will cause an error in the fitted lattice parameters. Since the samples were not moved during the diffraction experiments, this error will affect all measurements for a given sample, and for a given heating or cooling run, in the same way; i.e., it will result in a systematic upward or downward shift of the lattice parameter versus temperature plot. The estimated lattice parameter errors are reported in Table 2.

It will be assumed in the following work that the absolute error on the lattice parameters, i.e., that of the position of the trend lines, will be due to the error in the sample−detector distance. On the other hand, the error in each individual point within the trend will be the value reported by the Rietveld refinement procedure, which will result from statistical fluctuations in the number of X-rays detected (see next section).

2.4. Data Reduction and Refinement. The raw data, comprising 2-dimensional SAXS and WAXD patterns, were corrected for geometrical distortions within the area detectors. Detector tilt corrections were applied to adjust for slight misalignments, using the in-house Fit2D software package.[30] The beam center was monitored for each sample over each high temperature excursion, but no resolvable displacements were observed. After the geometric corrections were applied, 1-D scattering patterns were obtained by integrating the 2-D pixel images over the full 360° azimuthal range using the same program (Fit2D). Typical integrated 1-D diffraction patterns are shown in Figure 1.

The 1-D WAXD patterns were analyzed with the Rietveld method,[31,32] using the GSAS program[33] (see Supporting Information). A careful inspection of the data showed that all the observed Bragg reflections could be indexed with an orthorhombic unit cell. For each pattern collected, the systematic absences suggested the space group *Pnam* which, as indicated above, is the standard space group for polyethylene. Therefore, the orthorhombic polyethylene structure of Bunn[10] was used as the starting model for the refinements. Generally, at least 37 reflections were considered in each refinement. An example of a refined fit is included in Figure 1a. Typical errors in the cell parameters resulting from the Rietveld refinement process are quoted in Table 2. It can be seen that the refinement errors are significantly smaller than the sample placement errors.

2.5. Peak Asymmetry Corrections. A careful examination of the crystalline (110) and (200) peak shapes in the 1-D powder diffraction patterns indicated that there was some slight asymmetry present. This had the effect that the *a* and *b* lattice parameters obtained from the (110) and (200) reflections alone, i.e., using the range $6° < 2\theta < 9°$ (3.3 Å < *d* < 4.9 Å), were not consistent with those produced from the higher order reflections, i.e., using the range $9° < 2\theta < 24.7°$ (1.2 Å < *d* < 3.3 Å). Indeed, it was noticed that the trends in lattice parameters obtained from the two separate parts of the diffraction patterns started to diverge above ~60 °C (see Figure 2). The difference was most pronounced in the three shortest extended chain alkane crystals, $C_{102}H_{206}$, $C_{122}H_{246}$, and $C_{162}H_{326}$, appearing as a sharp kink in the *b* lattice parameter trend when calculated from the (110) and (200) reflections (dash-dotted line) compared to the trend determined from the remainder of the pattern (dotted line). This difference was interpreted as indicating that the peak profile function is not fitting the first two reflections sufficiently accurately to give consistency across the pattern at all temperatures; the large integrated intensity of the first two reflections means that small errors in the peak shapes will tend to dominate the fit with the remainder of the pattern.

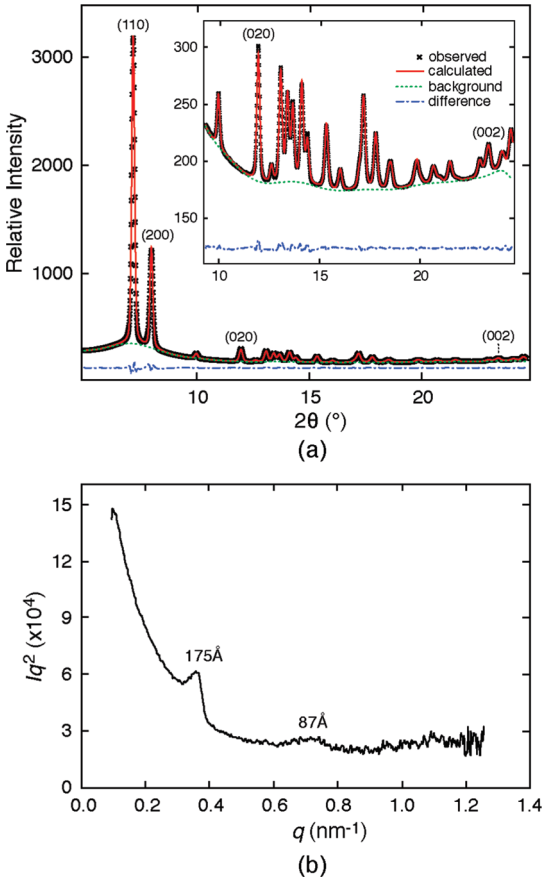

Figure 1. Typical experimental diffraction data for once-folded $C_{294}H_{590}$ (sample C294:1f) at 25 °C. (a) Wide-angle data (crosses). The refined plot is also shown (solid line) together with the background fit (dotted line) and difference plot (dashed-dotted line). (b) The corresponding small-angle data. The peak positions indicate a slightly smaller lamellar thickness than might be expected for chains of this length, which is suggestive of some degree of chain tilting within the lamellae.

It is interesting to note that this peak asymmetry has also been observed in other work involving refinements of polyethylene data, most noticeably in a branched polyethylene study performed by Baker and Windle[34] and in the work of Sajkiewicz et al.[35] considering crystallization on cooling from the melt. In order to resolve this data fitting problem, a peak-asymmetry parameter was included in the profile function during the refinement, as used previously by Caminiti et al.[36] This successfully resolved the issue, producing a better fit to the (110) and (200) reflections, and consistency across the whole pattern at all temperatures (see Figure 2, solid line). The physical origins of the peak asymmetry term and the implications of its use in the structural analysis of the *n*-alkanes will be discussed further below.

3. Results

3.1. Trends within Lattice Parameters. The lattice parameters for each of the *n*-alkane samples are shown in Figure 3 as a function of temperature. For convenience, they are grouped according to the initial number of folds present in the molecules. The lattice parameters are also tabulated, in 5 °C intervals, in Tables S2, S3, and S4 of the Supporting Information. Comparing the different sets of lattice parameters, it is clear that the variations in trend between the different crystal forms are quite subtle, with all samples

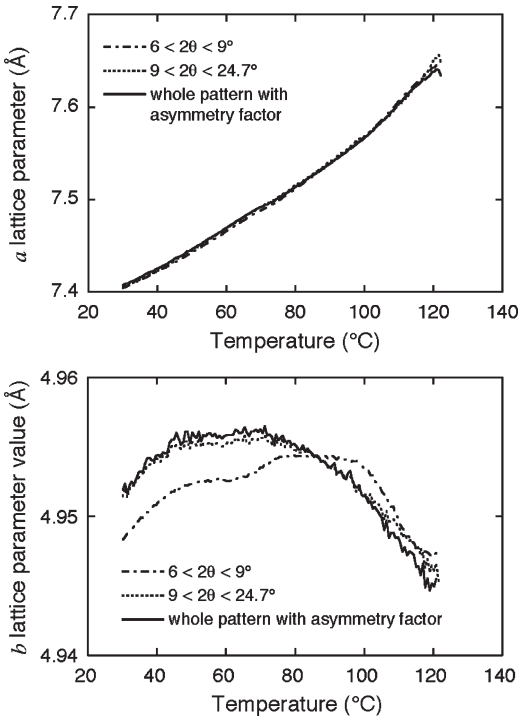

Figure 2. Plots demonstrating the effect of peak asymmetry on the *a* and *b* lattice parameters for an extended chain $C_{122}H_{246}$ sample. The results for a fit to the (110) and (200) peaks (data in the range $6° < 2\theta < 9°$, dash-dotted line) and for a fit to the higher angle peaks (data in the range $9° < 2\theta < 24.7°$, dotted line) are shown and compared with results for whole-pattern fitting, employing the peak asymmetry correction suggested by Caminiti et al.[36] (solid line).

showing the same overall behavior. Figure 4 shows similar sets of data for the branched alkanes and for Rigidex 50.

The diffraction patterns collected for the extended chain $C_{102}H_{206}$ and $C_{122}H_{246}$ had rather poor intensities compared with the other samples due to a combination of preferred orientation in the sample and low sample volume. As a consequence of this, the refined values for these samples were more noisy than for the other materials. This is particularly noticeable in the *c* lattice parameter plots. The once-folded $C_{198}H_{398}$ sample was contaminated with aluminum from the DSC pan, and this led to extra reflections in the diffraction pattern. These covered several of the higher order alkane reflections and made fitting of the *c* lattice parameter more problematic, as is apparent from the noisiness of that trace in Figure 3b.

The most obvious feature of all the samples is that the thermal expansion shown by the *a* lattice parameter is much greater than that seen in *b* or *c*. Thus, the thermal expansion of the *a* lattice parameter with temperature can be more or less regarded as the thermal expansion of the unit cell itself. Typically, the *a* parameter expands by about 0.25 Å (3.4%) over the temperature range measured (around 100 °C), whereas *b* expands by about 0.01 Å (0.2%) over the first 50 °C and then contracts by a similar amount before melting, and *c* shows an overall contraction of between 0.002 and 0.004 Å (0.08 to 0.16%), depending on the sample.

Looking at the lattice parameters for all the extended chain crystals, the $C_{102}H_{206}$ and $C_{122}H_{246}$ show a slightly different variation in the *b* and *c* lattice parameters compared to the other, longer chain crystals. In both cases, the parameters are significantly higher than those of the longer *n*-alkanes between room temperature and 100 °C. This may be because the chain ends at the lamellar surface occupy a greater volume fraction in these samples and thus have a greater influence on the bulk of the crystal. In fact, the general trend is for *b* and *c* to decrease with increasing chain length, with the implication that the lamellar surfaces lead to a less dense packing of the chain ends compared with the bulk, which in turn leads to a slight surface-induced expansion of the unit cell.

When examining the plots of the crystalline *a* parameters, the most obvious feature, apart from thermal expansion, is the stepwise change which occurs at elevated temperatures, as the chains unfold (see insets to Figure 3). This was previously reported by Terry et al.[26] The changes in fold state were confirmed using the SAXS data. As noted previously, each unfolding transition is accompanied by a reduction in the *a* parameter, i.e., an increase in density. The changes in *b* lattice parameter during unfolding are also apparent from Figure 3, but any stepwise changes in *c*, if they occur, are harder to discern. All folded *n*-alkanes demonstrate similar traits. In each case, when the lamellae thicken the *a* and *b* lattice parameters contract, with no obvious corresponding change in *c*. The density increases for each of the transitions highlighted in Figure 3 are shown in Table 3. It can be seen that the density changes are typically in the range 0.3−0.4%. The smaller change seen for the $C_{390}H_{782}$ 2f → 1f transition is probably due to there being a greater degree of disorder in this case because the material is initially crystallized in the thrice-folded state.

It is worth noting that, at the elevated temperatures required for chain unfolding, evidence for chain tilting within the lamellae is observed in the SAXS data, i.e., the lamellar thickness reduces, suggesting that the alkane chains are no longer normal to the lamellar surfaces. This has also been noted by de Silva et al.[3] We will examine this feature in more detail in a future publication.

Studying the lattice parameter traces for the branched alkane samples with temperature (Figure 4a) shows that the materials display the same trends as the linear *n*-alkane crystals. However, there is no lattice contraction prior to melting. This implies that neither branched system unfolds, with the system melting completely rather than thickening. This is confirmed by the SAXS data. The material with the butyl branches has a slightly more expanded lattice than that with methyl branches, which may be attributed to packing constraints of the butyl groups at the lamellar surfaces. In general, it is seen that the lattice parameter trends of the Rigidex 50 sample (Figure 4b) are very similar to the alkane crystals. However, at and above the temperature where significant crystal thickening is expected to start, the *a* lattice parameter in Rigidex 50 reaches a plateau. The mean lamellar thickness of the Rigidex 50 sample is 120 Å, which is comparable to once-folded $C_{198}H_{398}$.

3.2. Dependence of Lattice Parameters on Fold State. The most interesting aspect of the present study is to see how the variations in lattice parameter relate to the fact that the chain length and number of folds in the chain are exactly defined. On comparing samples with the same lamellar thickness but different numbers of folds, the clearest trends are observed in the *a* lattice parameter (Figure 5). It is seen that the materials with the same lamellar thickness, i.e., extended $C_{102}H_{206}$ compared with once-folded $C_{198}H_{398}$ and extended $C_{122}H_{246}$ compared with once-folded $C_{246}H_{494}$, take very nearly the same *a* lattice parameter value up to a temperature around 70 °C. Beyond this point the material containing folded chains begins to expand at a greater rate than the extended-chain material. However, the *a* parameter of the initially once-folded material becomes very close to the value of the equivalent material prepared in the unfolded state, once the

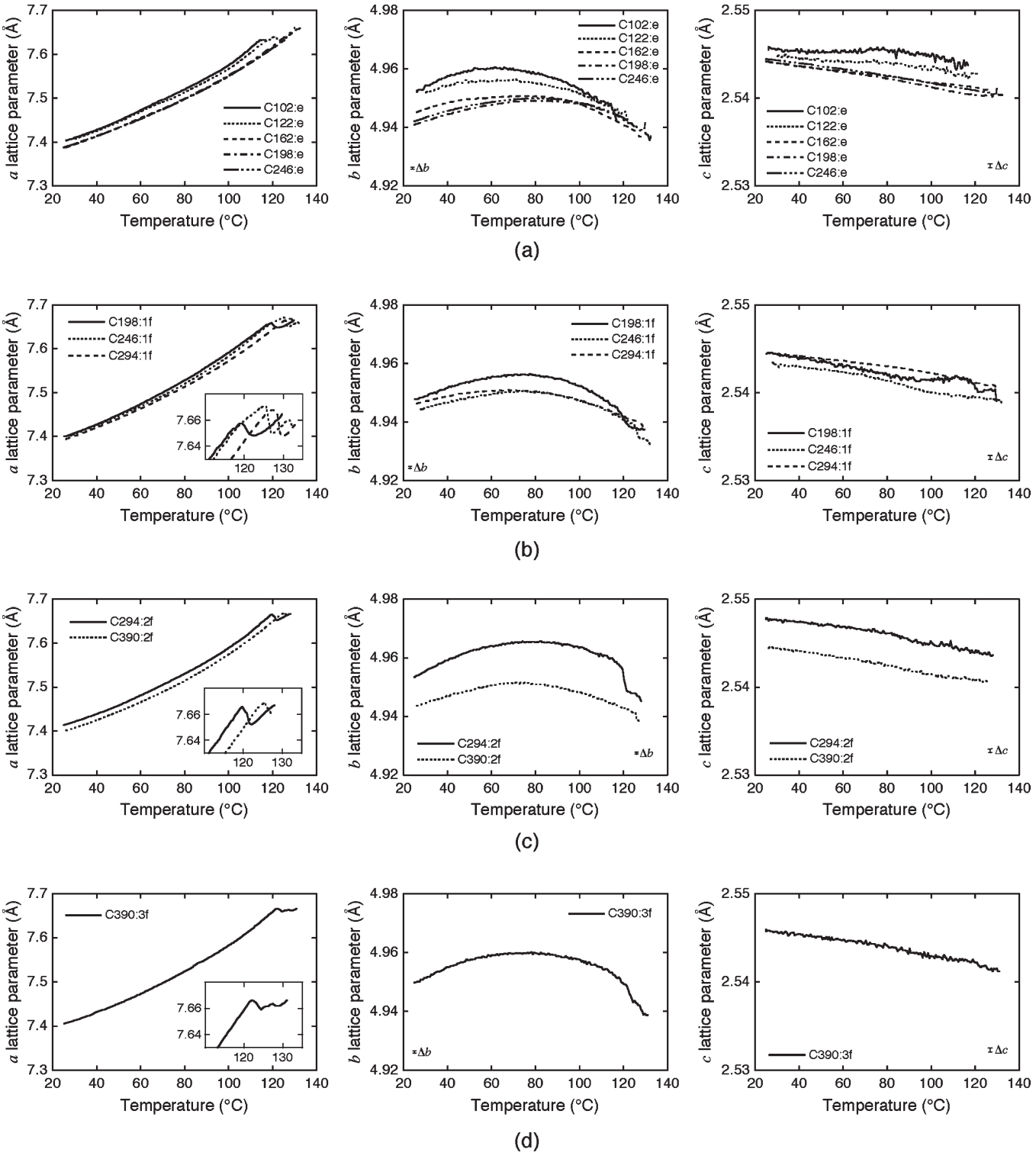

Figure 3. Lattice parameters versus temperature for all *n*-alkanes under consideration: (a) extended chain, (b) once-folded, (c) twice-folded, and (d) thrice-folded samples. The insets highlight the unfolding transitions. The magnitudes of the sample placement errors (Δb and Δc) are indicated on the plots. Δa is not shown because it is too small to see.

former material unfolds. For example, in Figure 5a at around 125 °C the once-folded $C_{246}H_{494}$ unfolds to give an *a* parameter equivalent to that of the extended chain material, while in Figure 5b the same effect is seen in $C_{198}H_{398}$ at 120 °C. A similar change is also seen in Figure 5c where twice-folded $C_{294}H_{590}$ unfolds to give an equivalent *a* parameter to the once-folded material. The divergent behavior at around 70 °C may be due to the occurrence of a relaxation process in the folded crystalline phase which may also be linked to the onset of chain tilting in the lamellae. This possibility will be discussed further below.

3.3. Dependence of Lattice Parameters on Lamellar Thickness. As discussed above, when comparing the variations in the *a* lattice parameter with temperature, the trends are very similar between materials with the same lamellar thickness. To examine this relationship further, Figure 6 shows plots of

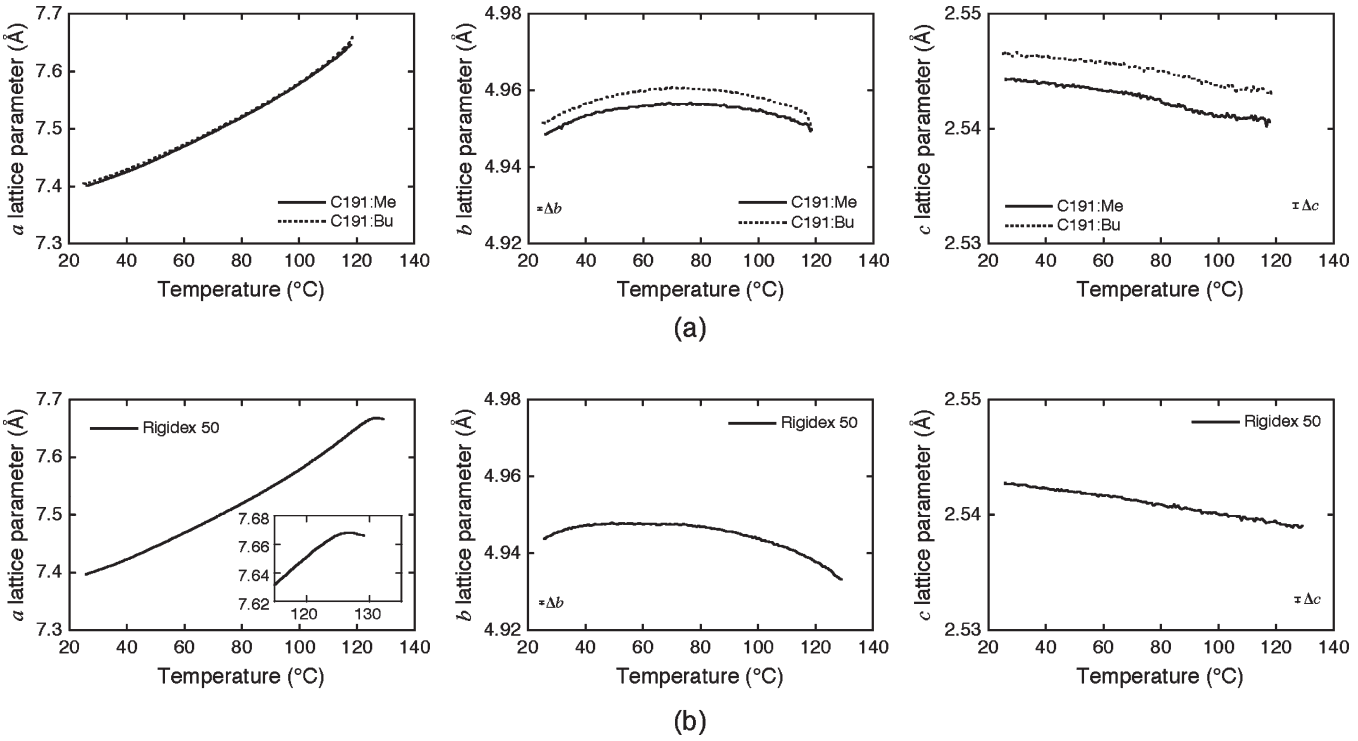

Figure 4. Lattice parameters versus temperature for (a) the branched alkanes and (b) the sample of Rigidex 50. The inset highlights the crystal thickening process in Rigidex 50 close to the melt.

Table 3. Density Increases Observed during Unfolding Transitions

material	transition	density increase, $\Delta\rho$ (%)
$C_{198}H_{398}$	1f → e	0.33
$C_{198}H_{398}$	1f → e	0.37
$C_{294}H_{590}$	2f → 1f	0.34
$C_{390}H_{782}$	3f → 2f	0.28
$C_{390}H_{782}$[a]	2f → 1f	0.10

[a] Initially three times folded.

the *a* lattice parameter versus the inverse of the lamellar thickness, for a range of temperatures. At each temperature an approximately linear relationship is seen, as indicated by the line of best fit. In other words, and in agreement with the findings of Davis et al. for polyethylene,[22,23] the thickest crystals have a more contracted lattice and the thinner crystals have a more expanded lattice. Thus, when a particular *n*-alkane has fewer folds, it forms thicker lamellae and its lattice tends to be more contracted. The values for Rigidex 50 and the branched alkanes are included in the figure and agree with the general trend.

In the plots, only the *a* lattice parameter is considered because, as discussed above, it is found to be the most receptive lattice parameter to temperature. In each case, the room temperature lamellar thickness is plotted to avoid any confusion caused by chain tilting at elevated temperature; apart from this effect, the lamellar thickness is generally quite insensitive to temperature.

3.4. Crystallization Experiments. Following the method described in section 2.2, an in situ WAXD study was performed on the *n*-alkane $C_{246}H_{494}$ during melt crystallization in order to see whether any explicit changes occurred in the unit cell during the initial crystallization period, which might provide insights into the mechanisms operating. The material was monitored as it crystallized both during a slow cool from the melt and isothermally.

The lattice parameters extracted from the slow cooling experiment are displayed in Figure 7a (solid line). Only the *a* parameter is shown since, as mentioned previously, this is the parameter displaying the most obvious trends. The results of the subsequent heating run are plotted on the same axes (dotted line). The results at each temperature for heating and cooling are very similar, suggesting that we are only observing the effects of thermal expansion.

Previous workers have monitored the lamellar thickness of $C_{246}H_{494}$ during melt crystallization using SAXS and found that, below the temperature range of extended chain growth (i.e., below about 121 °C), the initial lamellar period was a noninteger fraction of the full chain length which depended on the crystallization temperature and time.[7] These noninteger folded (NIF) lamellae subsequently transformed isothermally over several minutes either by thickening into an extended chain form or by thinning into a once-folded form. Further study indicated that the NIF form is actually one-third amorphous, with some chains integrally folded while others are not folded at all but traverse the crystal layers.[28] These latter chains are only partially crystalline.

Therefore, when cooling below 121 °C in Figure 7a, we surmise that the crystals forming are initially in the metastable NIF form. There is, however, no indication of any change in the cell parameter during transformation of the NIF to the extended or folded forms.

In a second experiment, isothermal crystallization is performed at 128.1 °C (see Figure 7b). This is toward the upper temperature limit for the growth of extended chain crystals. It is seen that the *a* lattice parameter starts off at a high value of 7.6515 Å but drops, after about 3 min, to 7.6485 Å, i.e. a drop of 0.003 Å, which is very small but significant when compared to the magnitude of the random errors in the measurement (±0.0004 Å, see Table 2). Both the *b* and *c* lattice parameters increase slightly over the same time period (not shown), but the net effect is a density increase of 0.006%, which may be attributed to the crystal annealing and perfecting. Over the remainder of the experiment, the *a* lattice parameter increases very slightly, which may be due

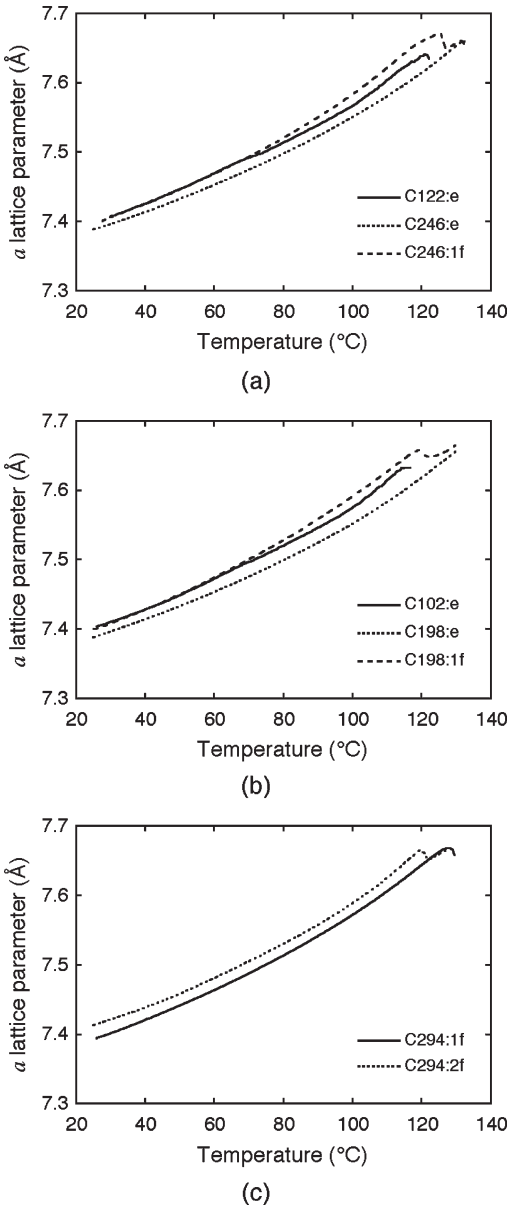

Figure 5. Trends in the *a* lattice parameter for samples with similar lamellae thicknesses: (a) once-folded $C_{246}H_{494}$ compared with chain-extended $C_{122}H_{246}$ and $C_{246}H_{494}$; (b) once-folded $C_{198}H_{398}$ compared with chain-extended $C_{102}H_{206}$ and $C_{198}H_{398}$; (c) twice-folded $C_{294}H_{590}$ compared with once-folded $C_{298}H_{590}$.

to changes in the crystal size distribution, as the sample anneals.

4. Discussion

As described above, we have performed a comprehensive survey of the lattice parameters of a range of ultralong *n*-alkanes as a function of temperature, from ambient conditions up to the melt. A number of conclusions may be drawn concerning these materials, which all crystallize in the same orthorhombic space group as polyethylene (*Pnam*). First, and most obviously, all samples showed extreme anisotropy in their thermal expansion, with significant expansion taking place on heating parallel to the *a* lattice direction, little net change in the *b* direction, and a slight contraction in the *c*, chain axis, direction. There are differences in the absolute values of these parameters between the samples, but the trends in all cases are very similar. The most obvious variations occur in the *a* parameter, and it is clear that the main

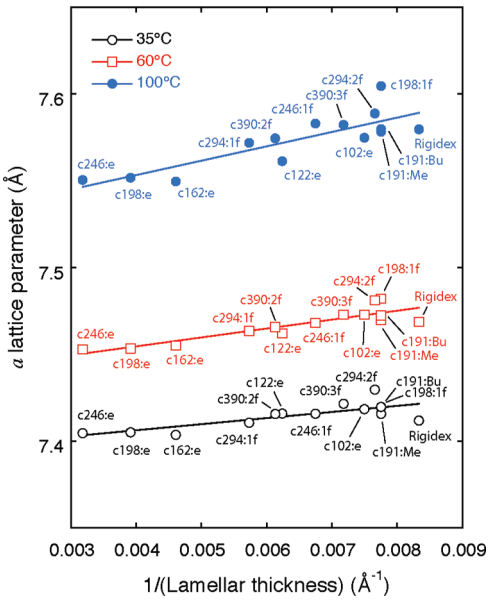

Figure 6. Trends in the *a* lattice parameter with inverse lamellar thickness at (a) 35, (b) 60, and (c) 100 °C. The solid line shows a line of best fit in each case. The errors in lattice parameter are smaller than the symbols plotted.

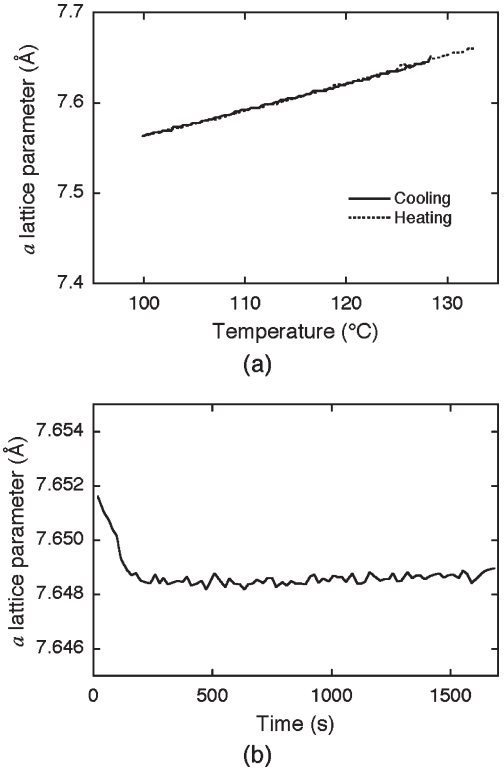

Figure 7. (a) Refined values of the *a* lattice parameter determined during melt crystallization of $C_{246}H_{494}$. The material is cooled from the melt (solid line) at 1 °C/min to 100 °C and subsequently heated at 2 °C/min (dotted line). (b) Refined values of the *a* lattice parameter determined during the isothermal crystallization of $C_{246}H_{494}$ at 128.1 °C.

trends are (1) for *a* to decrease with increasing chain length and (2) for *a* to increase with increasing number of folds in the molecules; i.e., *a* increases with decreasing number of backbone carbon atoms between the fold surfaces. Such is the dominance of the *a* parameter that the observed changes equate directly to changes in sample density.

The second conclusion which may be drawn is that the lattice contracts when, at elevated temperature, samples of folded *n*-alkanes undergo unfolding transitions. This is a corollary to the observations in the previous paragraph. For, as shown in Figure 5, when folded material transforms to a less folded state, the resulting lattice parameters are close to those of samples initially prepared in that state.

The behavior described is clearly a consequence of the influence of the top and bottom surfaces of the crystalline lamellae and the presence at those surfaces of chain folds and chain ends. In the case of the extended chain crystals, the influence of the chain ends must diminish as the lamellae become thicker. From the results shown in Figure 3a, it is apparent that the limiting behavior is reached for $C_{162}H_{326}$; the lattices of $C_{102}H_{206}$ and $C_{122}H_{246}$ are expanded relative to $C_{162}H_{326}$, whereas the *a* lattice parameter curves for $C_{162}H_{326}$, $C_{198}H_{398}$, and $C_{246}H_{494}$ are all superimposed.

The influence of chain folds is similar to that of chain ends; i.e., they lead to lattice expansion. However, this statement requires some qualification, as systems exist in which the opposite effect occurs. For example, in a study of hydroxybutyrate oligomers, Li et al. observed that chain folds led to a small contraction of the crystal lattice in the (110) fold direction, of ca. 0.2%.[37] This difference in behavior may be related to the cross-sectional area occupied by the chain-fold compared with that of the chain stems. In the case of the hydroxybutyrate oligomers, the backbone forms a 2_1 helix,[38] which is comparatively wide compared with the space required by a fold. On the other hand, the regular planar zigzag of the *n*-alkane backbone is able to pack more densely than a defect-rich fold. As a result, chain folds tend to pull the hydroxybutyrate chain stems closer together, while pushing *n*-alkane chain stems further apart. The ability of chain folds and other conformational defects such as jogs to produce lattice expansion in long *n*-alkanes has been demonstrated using computer simulations.[18]

As well as affecting the lattice parameters, the chain ends and chain folds may play a role in creating the peak asymmetry observed in the 1-D powder diffraction patterns, as noted in section 2.5. There are several possible explanations for this asymmetry.

One explanation relates to the possible presence of a second orthorhombic phase within the pattern, closely overlaid on the first. This may originate from the lamellar surfaces which, due to the chain ends and folds, occupy an orthorhombic lattice slightly enlarged in comparison to the bulk. Such a model was postulated by Baker and Windle to explain a similar observation in a branched polyethylene sample.[34] A second option is that the effect might be associated with a poor fit to the amorphous scattering, for example beneath the (110) and (200) reflections, which might adversely affect the shapes of these dominant diffraction peaks (a typical background curve is shown in Figure 1a). A third possibility is that there could be anisotropic paracrystalline disorder, which would amount to an uneven distribution of lattice spacings across the sample. This would lead to anisotropic broadening of the reflections in reciprocal space, which could in turn lead to peak asymmetry when powder averaging was performed.

Each argument is feasible, but it is not possible to distinguish between them in this work. However, since the effect is most pronounced in the three shortest *n*-alkane crystals, i.e., those with minimal amorphous component and which might be expected to form the most regular crystals, it would appear that the first explanation, involving superposition of diffraction from two or more phases, is the most likely of those discussed. In fact, there are other possible causes of the anomalous data which should also be considered, including crystallographic defects such as vacancies, dislocations, and grain boundaries at which the chains twist as they cross. It is fortunate that the diffraction data are sufficiently high resolution that they could be used to evaluate such possibilities; a detailed model of the crystal disorder may be constructed to replicate the diffraction data more closely, and this will form the subject of future work.

The supposition for the present, however, is that the chain ends in the extended chain crystals exert an influence on the chain packing, local to the lamellar surfaces, such that the unit cells in this region are more expanded than those in the bulk. This implies that the crystals must be distorted in some way or else that there must be some other means to relieve the strain in the region of the crystal surface, such as vacancies or other lattice disorder. In line with our observations, the effect should be more pronounced for the shorter *n*-alkanes, where the surface regions comprise a larger volume fraction of the crystal. Curiously, the peak asymmetry appears less pronounced for the chain-folded crystals. However, the widths of the (110) and (200) diffraction peaks are greater in the chain-folded crystals than in the extended chain cases, implying that the chain-folded crystals are more disordered, and we speculate that this effect is tending to mask any asymmetry which might be induced by the lamellar surfaces.

A further implication of the above discussion is that each sample does not possess unique lattice parameters, but a range of values. However, since there is no way to separate the different contributions, the best that we may achieve is to apply the asymmetry correction and treat the scattering as if it comes from a single phase, with a single set of lattice parameters, accepting that these will, in fact, be complicated averages taken over the whole of the crystalline lamellae.

The anomalous thermal expansion behavior shown in Figure 5 is also worth further consideration. In this figure it was observed that samples with the same stem length but different fold states, e.g., sample C122:e compared with C246:1f or sample C102:e compared with C198:1f, showed the same thermal expansion in their *a* parameters up to ca. 70−80 °C, above which their behaviors diverged, the folded materials expanding more rapidly than the equivalent extended chain materials. Initially, it was thought that the presence of a fold would be more likely to pin the chains together and suppress any thermal expansion. However, this is clearly not the case, and just as the presence of chain folds leads to an increased *a* parameter for a given lamellar thickness, so it also promotes a greater thermal expansion in that parameter, but only when the temperature is greater than ca. 70 °C. This temperature happens to coincide with the onset of the well-known α process in polyethylene.[39,40]

In polyethylene, the α process has two components, one relating to the crystalline phase and the other to the amorphous. The crystalline relaxation, which may be observed in dielectric studies of suitably decorated materials[41,42] as well as using NMR,[43−46] consists of 180° rotational jumps of the chain stems, accompanied by a translation by one methylene group along the *c* axis that leaves the chain in crystallographic register. The activation energy for this process is in the range 100−120 kJ mol^{-1}. By this means, there is chain transport through the crystal, which unpins the amorphous sequences at the crystal surface and allows the crystalline relaxation to couple to the amorphous relaxation. The amorphous relaxation, on the other hand, is a mechanically activated process, involving reorganization of the chain in the amorphous phase.[47] It seems likely that similar α processes are occurring in the ultralong *n*-alkanes and over a similar temperature range.

There have been two NMR studies of the ultralong *n*-alkanes to date. Klein and Driver studied samples of $C_{198}H_{398}$ and $C_{246}H_{494}$, as well as the methyl and butyl branched alkanes considered here, using ^{13}C NMR at 60 °C.[48] Their samples were not in well-defined fold states, being produced by a rapid quench from the melt followed by annealing. They concluded

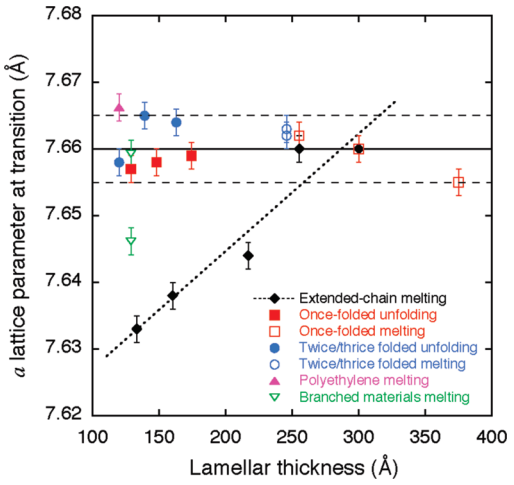

Figure 8. A summary of the *a* lattice parameters plotted against lamellar thickness at the melting and unfolding transitions of all the materials being considered.

that longitudinal chain diffusion was indeed occurring, although they questioned whether the alkanes could reptate around the folds, suggesting, instead, that diffusion led to an exchange between the crystalline and amorphous phases through changes in the length of chain involved in each fold. Very recently, Grasso and Titman have performed a detailed ^{13}C NMR analysis of chain-extended and once-folded samples of $C_{246}H_{494}$.[49] These latter authors note the occurrence of the α process, suggesting it has a lower activation energy than in polyethylene. Unlike the previous authors, Grasso and Titman conclude that the fold does not provide a barrier to chain diffusion, which they attribute to the fact that their samples are more regular, and with tighter folds, than the earlier work. They also provide a direct measurement of the size of the fold region in once-folded $C_{246}H_{494}$, which includes ~8 carbon atoms.

It is interesting to note that the onset of chain tilting in the lamellae occurs in the same temperature range as the α process.[3] This is possibly not surprising since chain tilting will also require chain mobility. Therefore, it appears that, at the temperature at which the thermal expansions begin to differ, i.e., at around 70−80 °C, the anomalous thermal expansion and the onset of chain tilting are linked to the activation of the α process and the consequent chain mobility that this endows. The fact that the chain-folded crystals expand more than the chain-extended ones may be related to the greater free volume associated with the folds and to an exchange of material between the chain stems and folds, which cannot occur in the extended-chain case.

An examination of the trends in lattice parameters for the various samples shows that the *a* lattice parameter always appears to take similar values (in the range 7.63−7.67 Å) immediately before the lamellae thicken or melt. Probing this observation further by extracting the values of *a* just prior to these transitions and plotting them against lamellar thickness reveals some interesting trends, as displayed in Figure 8. In the case of the extended-chain materials, it is seen that an approximately linear relation exists between the *a* lattice parameter just prior to melting and the lamellar thickness (Figure 8, dotted line). However for almost all of the other samples considered, the value of the *a* lattice parameter on melting or unfolding takes a value in the range 7.660 ± 0.005 Å, which is independent of chain length, crystal type, or lamellar thickness. The only exception to this behavior is the methyl-branched material, which falls outside the range at 7.646 Å.

These results suggest that, for the material to melt, the lattice must reach a certain critical dimension. With the exception of the extended-chain crystals, this appears to occur when $a \approx 7.66$ Å. This value appears to mark an upper limit to the free volume in the unit cells of the *n*-alkanes, above which the crystals cease to be stable. We use the term "melt" here to refer both to normal melting and to the unfolding transitions, as it appears the latter involves simultaneous melting of the shorter, folded crystals and recrystallization into the more extended state. Notably, when slow cooling from the melt, the first crystals appear at 128.4 °C with lattice parameter 7.6513 Å (Figure 7a) while isothermal crystallization at 128.1 °C (Figure 7b) leads to an initial crystal population with $a = 7.6515$ Å. In both cases, the crystal dimension is a little less than the hypothetical critical value of 7.66 Å; i.e., the crystal initially grows with a density that is just greater than the minimum possible to remain stable. It is also worth noting that the *a* parameter of Rigidex 50 reaches a plateau at ca. 7.667 Å, where the crystals are thickening continuously, and then ultimately melts without any further expansion.

In considering the melting of the folded materials, we might invoke the theory of Lindemann,[50] who suggested that a crystal melts when the amplitude of molecular vibration exceeds a critical fraction of the distance between neighboring molecules. In the present case we consider the behavior of the *a* parameter only, since most thermal motion and expansion is in that direction. Since the bulk of the chain stems are in very similar environments and melt at similar *a* values, we might expect, following Lindemann, that all samples will possess similar rms thermal displacements parallel to the *a* axis when they melt. In fact, a review of the thermal motion parameters derived from the Rietveld fits is rather inconclusive, with rms values in the range 0.3−0.4 Å, and no obvious correlation with the *a* parameter at melt. Instead of pursuing this approach, we turn to a more sophisticated theory.

In the case of the extended-chain *n*-alkanes, the Flory−Vrij approach to crystal melting has been very successful.[51] Flory and Vrij suggested treating the melting process in two steps: in the first, the chain assumes a disordered conformation and melt density but preserves the intermolecular pairings of end groups while, in the second, the end-group pairing is broken, allowing the chain ends to diffuse at random through the melt. This analyis leads to

$$\left(\frac{n\Delta H}{R}\right)\Delta T - \left(\frac{n\Delta C_p}{2R}\right)(\Delta T)^2 - T_m T_m^0 \ln n \cong \left(\frac{T_m^0}{R}\right)(T_m \Delta S_e - \Delta H_e) \quad (1)$$

where *n* is the chain length and ΔT the undercooling. Equation 1 contains five experimental parameters: the enthalpy of fusion per CH_2 group, ΔH, the enthalpy and entropy of fusion of the end groups, ΔH_e and ΔS_e, the change in heat capacity on melting, ΔC_p, and equilibrium melting temperature, T_m^0. Flory and Vrij obtained a good fit to the available experimental data for $11 \leq n \leq 100$ using the values $\Delta H = 3.975$ kJ mol^{-1}, $\Delta H_e = -8.996$ kJ mol^{-1}, $\Delta S_e = 10.25$ J K^{-1} mol^{-1}, $\Delta C_p = 4.184$ J K^{-1} mol^{-1}, and $T_m^0 = 145.4$ °C.

The predictions of eq 1 for T_m are shown in Figure 9 for $n \leq 400$ (solid curve). Also shown are the melting temperatures determined for the linear alkanes from the WAXD data (solid circles). It is immediately clear that the extended-chain materials fit the Flory−Vrij prediction closely. The slight discrepancies in each case are probably due to inadequacies in the measurement method; i.e., the melting point was determined from the WAXD traces rather than from a DSC endotherm.

Equation 1 was specifically intended for predicting the melting points of extended-chain crystals, in which all molecules are the same length, and is not suited to the treatment of folded *n*-alkanes or polydisperse polymers.[52] However, we may incorporate the

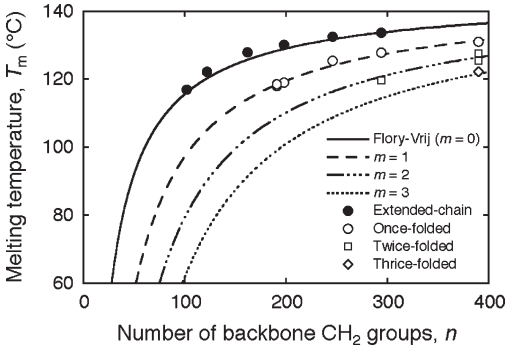

Figure 9. Curves showing the melting temperature versus number of backbone carbon atoms, n, as calculated from the Flory−Vrij equation (eq 1, solid line) and from the modified Flory−Vrij equation (eq 2, broken lines) described in the text, for m = 1, 2, and 3 folds. Experimental data are included as discrete points.

effects of chain folds through an additional free energy term, ΔG_f, per fold. It is assumed that each unfolding transition consists of melting followed by recrystallization; we are concerned with the first part of this process. ΔG_f appears as additional terms on the right-hand side of eq 1, i.e.

$$\left(\frac{n\Delta H}{R}\right)\Delta T - \left(\frac{n\Delta C_p}{2R}\right)(\Delta T)^2 - T_m T_m^0 \ln n \cong \left(\frac{T_m^0}{R}\right)[T_m(\Delta S_e + m\Delta S_f) - (\Delta H_e + m\Delta H_f)] \quad (2)$$

where ΔS_f and ΔH_f are the entropy and enthalpy change on melting per fold in the molecule. It is worth noting that several previous authors have considered the melting of folded chain molecules. In particular, the treatment of Buckley and Kovacs[53] is also related to the Flory−Vrij approach, as here, but was applied to the melting of integer-folded poly(ethylene oxide) molecules. The problem of crystallization and the onset of folding in the n-alkanes has been studied extensively by Hoffman.[54,55]

We obtain values for ΔS_f and ΔH_f empirically by performing least-squares fitting to the 10 transition temperatures available from the folded materials. In fact, because of the range of n over which data are available, there are many combinations of ΔS_f and ΔH_f which fit equally well, the differences appearing for $n < 100$, where no folded materials are available. Therefore, by way of illustration, we arbitrarily set $\Delta H_f = -10$ kJ mol^{-1} and obtain $\Delta S_f = 20.6$ J K^{-1} mol^{-1} from our fitting procedure. The resulting curves are shown in Figure 9, together with the experimental values, for m = 1, 2, and 3. It is clear that eq 2 produces a good fit to the transition temperatures of the once-folded materials (m = 1). The fits for m = 2 and 3 also appear reasonable, despite the small number of data points. It is interesting to note that the branched materials, C191:Me and C191:Bu, also lie on the curve for m = 1. Since it has not proved possible to form folded-chain crystals with fewer than about 150 carbon atoms in the backbone, the addition of branches may, in the future, provide a route to obtaining data for folded materials with smaller values of n.

The modified Flory−Vrij equation (eq 2) makes no predictions about the critical lattice dimension required for melting or unfolding. Also, no significance should be attached to the values of ΔH_f and ΔS_f used in Figure 9, which were mainly chosen for convenience. In the derivation of eq 2, no attempt is made to explain the physical origin of ΔG_f; a clearer picture of its origin would perhaps help to narrow the choices for ΔH_f and ΔS_f. However, despite these shortcomings, the modified Flory−Vrij equation appears useful as a way of accounting for the unfolding and melting temperatures of the ultralong n-alkanes.

5. Conclusions

This work has drawn on the fact that the ultralong n-alkanes form crystals with uniquely defined thicknesses and fold states in order to investigate the influence of these parameters on the dimensions of the crystal lattice. Highly precise lattice parameters have been determined as a function of temperature for a range of such n-alkanes, prepared in a variety of different fold states, and the observed trends reported. All samples behaved in a similar manner, with the dominant thermal expansion occurring parallel to the a cell axis and a small thermal contraction parallel to the chain axis (c axis). The general trends observed are that the lattice expands as the number of folds per chain increases, but contracts as the lamellar thickness increases. An approximate inverse relationship exists between the a parameter and the lamellar thickness, as previously found for polyethylene by Davis et al.[22,23] As noted previously, the folded alkanes undergo a sequence of unfolding transitions at elevated temperatures, which typically lead to density increases in the range 0.3−0.4%. It is found that the majority of unfolding and melting transitions occur when the a lattice parameter is in the range 7.660 ± 0.005 Å. However, no clear explanation is currently available for this observation. The extended-chain n-alkanes are found to melt at temperatures predicted by the well-known Flory−Vrij theory.[51] By incorporating an additional fold free energy into the Flory−Vrij equation, it has proved possible to account for the unfolding temperatures of both the n-alkanes and the branched systems. Anomalous thermal expansion behavior was observed in several folded crystals, beginning at ca. 70−80 °C. This has been attributed to the occurrence of an α relaxation, similar to that found in polyethylene, and will be examined further in a subsequent publication.

Acknowledgment. The authors thank Gerald Brooke and the EPSRC for providing materials, the EPSRC for financial support through a studentship, and the ESRF for supporting a studentship and for provision of synchrotron radiation facilities. They especially thank Jon Wright and Gavin Vaughan for assistance in using beamline ID11, and Pierre Panine and Peter Boesecke for their assistance with beamline ID2, on many occasions throughout this project.

Supporting Information Available: Further experimental details relating to sections 2.1, 2.3, and 2.4 as well as tables of lattice parameters versus temperature for all of the samples discussed in section 3. This material is available free of charge via the Internet at http://pubs.acs.org.

References and Notes

(1) Bidd, I.; Whiting, M. C. *J. Chem. Soc., Chem. Commun.* **1985**, No. 9, 543–544.
(2) Brooke, G. M.; Burnett, S.; Mohammed, S.; Proctor, D.; C, W. M. *J. Chem. Soc., Perkin Trans. 1* **1996**, No. 13, 1635–1645.
(3) de Silva, D. S. M.; Zeng, X.-B.; Ungar, G.; Spells, S. J. *Macromolecules* **2002**, *35*, 7730–7741.
(4) Hobbs, J. K.; Hill, M. J.; Barham, P. J. *Polymer* **2000**, *41*, 8761–8773.
(5) Hobbs, J. K.; Hill, M. J.; Barham, P. J. *Polymer* **2001**, *42*, 2167–2176.
(6) Organ, S. J.; Ungar, G.; Keller, A. *J. Polym. Sci., Part B: Polym. Phys.* **1990**, *28*, 2365–2384.
(7) Ungar, G.; Keller, A. *Polymer* **1986**, *27*, 1835–1844.
(8) Ungar, G.; Zeng, X. B.; Spells, S. J. *Polymer* **2000**, *41*, 8775–8780.
(9) Ungar, G.; Zeng, X. B. *Chem. Rev.* **2001**, *101*, 4157–4188.
(10) Bunn, C. W. *Trans. Faraday Soc.* **1939**, *35*, 482–491.
(11) Bunn, C. W. Molecular Structure. In *Polyethylene: The Technology and Uses of Ethylene Polymers*; Renfrew, A., Morgan, P., Eds.; Iliffe & Sons Ltd.: London, 1957; pp 81−120.
(12) Bunn, C. W.; Alcock, T. C. *Trans. Faraday Soc.* **1945**, *41*, 317–325.
(13) Hu, H.; Dorset, D. L. *Acta Crystallogr.* **1989**, *B45*, 283–290.

(14) Kavesh, S.; Schultz, J. M. *J. Polym. Sci., Part A-2: Polym. Phys.* **1970**, *8*, 243–276.
(15) Müller, A. *Proc. R. Soc. London A* **1928**, *120*, 437–459.
(16) Swan, P. R. *J. Polym. Sci.* **1962**, *56*, 403–407.
(17) Dorset, D. L.; Moss, B. *Polymer* **1983**, *24*, 291–294.
(18) Phillips, T. L.; Hanna, S. *Polymer* **2005**, *46*, 11003–11018.
(19) Phillips, T. L.; Hanna, S. *Polymer* **2005**, *46*, 11019–11034.
(20) Phillips, T. L.; Hanna, S. *Polymer* **2005**, *46*, 11035–11050.
(21) Gautam, S.; Balijepalli, S.; Rutledge, G. C. *Macromolecules* **2000**, *33*, 9136–9145.
(22) Davis, G. T.; Eby, R. K.; Colson, J. P. *J. Appl. Phys.* **1970**, *41*, 4316–4326.
(23) Davis, G. T.; Eby, R. K.; Matin, G. W. *J. Appl. Phys.* **1968**, *39*, 4973–4981.
(24) Magonov, S. N.; Yerina, N. A.; Ungar, G.; Reneker, D. H.; Ivanov, D. A. *Macromolecules* **2003**, *36*, 5637–5649.
(25) Sanz, N.; Hobbs, J. K.; Miles, M. J. *Langmuir* **2004**, *20*, 5989–5997.
(26) Terry, A. E.; Phillips, T. L.; Hobbs, J. K. *Macromolecules* **2003**, *36*, 3240–3244.
(27) Ungar, G.; Stejny, J.; Keller, A.; Bidd, I.; Whiting, M. C. *Science* **1985**, *229*, 386–389.
(28) Ungar, G.; Zeng, X. B.; Brooke, G. M.; Mohammed, S. *Macromolecules* **1998**, *31*, 1875–1879.
(29) Rastogi, A.; Hobbs, J. K.; Rastogi, S. *Macromolecules* **2002**, *35*, 5861–5868.
(30) Hammersley, A. P.; Svensson, S. O.; Thompson, A.; Graafsma, H.; Kvick, Å.; Moy, J. P. *Rev. Sci. Instrum.* **1995**, *66* (SRI-94), 2729–2733.
(31) Prince, E. In *The Rietveld Method*; Young, R. A., Ed.; Oxford Science Publications: Oxford, 1993.
(32) Rietveld, H. M. *J. Appl. Crystallogr.* **1969**, *2*, 65–71.
(33) Larson, A. C.; Von Dreele, R. B. General Structure Analysis System (GSAS), Los Alamos National Laboratory Report LAUR 86-748, **2004**.
(34) Baker, A. M. E.; Windle, A. H. *Polymer* **2001**, *42*, 667–680.
(35) Sajkiewicz, P.; Hashimoto, T.; Saijo, K.; Gradys, A. *Polymer* **2005**, *46*, 513–521.
(36) Caminiti, R.; Pandolfi, L.; Ballirano, P. *J. Macromol. Sci.* **2000**, *B39*, 481–492.
(37) Li, J.; Organ, S. J.; Terry, A. E.; Hobbs, J. K.; Barham, P. J. *Polymer* **2004**, *45*, 8937–8947.
(38) Cornibert, J.; Marchessault, R. H. *J. Mol. Biol.* **1972**, *71*, 735–756.
(39) Boyd, R. H. *Polymer* **1985**, *26*, 1123–1133.
(40) Boyd, R. H. *Polymer* **1985**, *26*, 323–347.
(41) Ashcraft, C. R.; Boyd, R. H. *J. Polym. Sci., Part B: Polym. Phys.* **1976**, *14*, 2153–2193.
(42) Boyd, R. H.; Yemni, T. *Polym. Eng. Sci.* **1979**, *14*, 1023–1028.
(43) Olf, H. G.; Peterlin, A. *J. Polym. Sci., Part A-2: Polym. Phys.* **1970**, *8*, 753–770.
(44) Olf, H. G.; Peterlin, A. *J. Polym. Sci., Part A-2: Polym. Phys.* **1970**, *8*, 771–789.
(45) Opella, S. J.; Waugh, J. S. *J. Chem. Phys.* **1977**, *66*, 4919–4924.
(46) Spiess, H. W.; Schmidt-Rohr, K. *Macromolecules* **1991**, *24*, 5288–5293.
(47) Illers, K. H. *Kolliod Z. Z. Polym.* **1969**, *231*, 622–659.
(48) Klein, P. G.; Driver, M. A. N. *Macromolecules* **2002**, *35*, 6598–6612.
(49) Grasso, G.; Titman, J. T. *Macromolecules* **2009**, *42*, 4175–4180.
(50) Lindemann, F. A. *Phys. Z.* **1910**, *11*, 609–612.
(51) Flory, P. J.; Vrij, A. *J. Am. Chem. Soc.* **1963**, *85*, 3548–3553.
(52) Mandelkern, L.; Stack, G. M. *Macromolecules* **1984**, *17*, 871–878.
(53) Buckley, C. P.; Kovacs, A. J. *Colloid Polym. Sci.* **1976**, *254*, 695–715.
(54) Hoffman, J. D. *Macromolecules* **1986**, *19*, 1124–1128.
(55) Hoffman, J. D. *Polym. Commun.* **1986**, *27*, 39–40.